

Excellence in Chemistry Research

Announcing our new flagship journal

- Gold Open Access
- Publishing charges waived
- Preprints welcome
- Edited by active scientists



Meet the Editors of *ChemistryEurope*



Luisa De Cola

Università degli Studi
di Milano Statale, Italy



Ive Hermans

University of
Wisconsin-Madison, USA



Ken Tanaka

Tokyo Institute of
Technology, Japan

Cooperativity-Driven Reactivity of a Dinuclear Copper Dimethylglyoxime Complex

Raphael I. Petrikat,^[a] Sophie T. Steiger,^[b] Elham Barani,^[c] Pit J. Boden,^[b] Maximilian E. Huber,^[b] Mark R. Ringenberg,^[d] Gereon Niedner-Schatteburg,^[b] Karin Fink,^[c] and Sabine Becker*^[a]

In memory of Prof. Dr. Markus Gerhards.

Abstract: In this report, we present the dinuclear copper(II) dimethylglyoxime (H₂dmg) complex [Cu₂(H₂dmg)(Hdmg)(dmg)]⁺ (1), which, in contrast to its mononuclear analogue [Cu(Hdmg)₂] (2), is subject to a cooperativity-driven hydrolysis. The combined Lewis acidity of both copper centers increases the electrophilicity of the carbon atom in the bridging μ₂-O=N=C-group of H₂dmg and thus, facilitates the nucleophilic attack of H₂O. This hydrolysis

yields butane-2,3-dione monoxime (3) and NH₂OH that, depending on the solvent, is then either oxidized or reduced. In ethanol, NH₂OH is reduced to NH₄⁺, yielding acetaldehyde as the oxidation product. In contrast, in CH₃CN, NH₂OH is oxidized by Cu^{II} to form N₂O and [Cu(CH₃CN)₄]⁺. Herein are presented the combined synthetic, theoretical, spectroscopic and spectrometric methods that indicate and establish the reaction pathway of this solvent-dependent reaction.

Introduction

The cooperative effect, that is, when two or more components achieve a desired reactivity often greater or inaccessible to either of the individual components, is widely found in chemistry and biological systems, for example, in catalysis, metalloenzymes, assembly of compounds on surfaces, and supramolecular polymerization to yield and/or control a desired chemical behavior.^[1–5] On a molecular level, for example, in a complex, cooperativity can occur due to metal–ligand, ligand–ligand, or metal–metal interactions. The coupling of metal centers in multinuclear complexes can influence the magnetic,

catalytic, and optical properties, which leads to a clear distinction in comparison to their mononuclear analogues.^[4,6–8] This cooperativity can either be of functional, enthalpic or entropic nature.^[9] Copper(II) dimethylglyoxime (H₂dmg) complexes are suitable for the investigation of such a cooperative effect because a variety of complexes differing in their composition are known. These complexes include mono-,^[10–12] di-^[12–15] and tetranuclear^[15,16] complexes, which have been characterized by crystal structure analysis,^[10–16] IR spectroscopy,^[11–13,16,17] UV/Vis spectroscopy,^[12–14,16,18] EPR^[19] and other magnetic methods.^[13,14,16] Additionally, mixtures of Cu^{II} salts and dimethylglyoxime have been applied in catalytic reactions such as the N-arylation of imidazole derivatives^[20] and the decomposition of hydrogen peroxide with subsequent oxidation of benzyl alcohol and ethylbenzene (zeolite encapsulated).^[21]

Due to our interest in multinuclear copper complexes and their reactivity,^[12,22] we focused on the dinuclear complex [Cu₂(H₂dmg)(Hdmg)(dmg)]⁺ (1) and its mononuclear analogue [Cu(Hdmg)₂] (2) as comparison (Figure 1). Two of the possible three isomers of 1 have been reported, whereas isomer I is predominant in literature^[13,14,16] and favored with increasing pH value.^[13] In this article, we report the cooperativity-driven and solvent-dependent degradation of copper-bound H₂dmg to either NH₄⁺ or N₂O.

Results and Discussion

Compound 1 was obtained by the reaction of Cu(ClO₄)₂·6H₂O and H₂dmg in ethanol and subsequent crystallization by pentane diffusion. Similarly, 2 was obtained by the reaction of Cu(OAc)₂·2H₂O and H₂dmg in methanol. Slow evaporation of the solvent led to crystallization. The molecular structures were

[a] R. I. Petrikat, Jun.-Prof. Dr. S. Becker
RPTU Kaiserslautern-Landau
Institut für Anorganische Chemie
Erwin-Schroedinger-Str. 54, 67663 Kaiserslautern (Germany)
E-mail: sbecker@chemie.uni-kl.de

[b] S. T. Steiger, P. J. Boden, M. E. Huber, Prof. Dr. Dr. G. Niedner-Schatteburg
RPTU Kaiserslautern-Landau
Institut für Physikalische Chemie
Erwin-Schroedinger-Str. 52, 67663 Kaiserslautern (Germany)

[c] E. Barani, Prof. Dr. K. Fink
Karlsruhe Institute of Technology (KIT)
Institute of Nanotechnology
Hermann-von-Helmholtz-Platz 1
76344 Eggenstein-Leopoldshafen (Germany)

[d] Dr. M. R. Ringenberg
Société Suisse des Explosifs,
Fabrikstrasse 48, CH-3900 Brig (Switzerland)

Supporting information for this article is available on the WWW under <https://doi.org/10.1002/chem.202203438>

© 2023 The Authors. Chemistry - A European Journal published by Wiley-VCH GmbH. This is an open access article under the terms of the Creative Commons Attribution Non-Commercial NoDerivs License, which permits use and distribution in any medium, provided the original work is properly cited, the use is non-commercial and no modifications or adaptations are made.

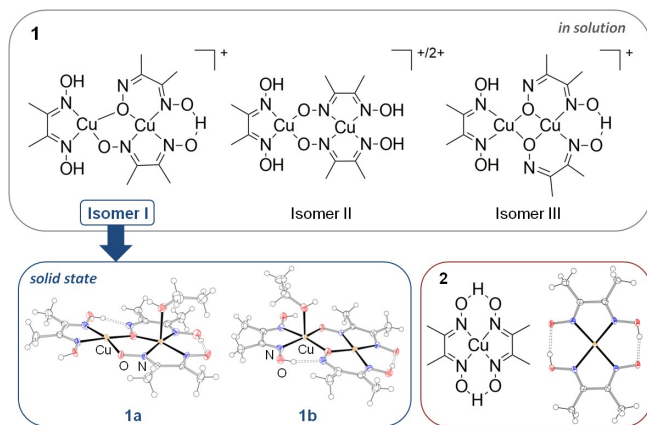


Figure 1. Top: structures of the three isomers of **1** in solution, anion and coordinating solvent molecules not shown for clarity. The charge of isomer II and the positions of the protons are not clarified, depending on the deprotonation state, the charge can be +1 or +2. Bottom: Molecular structures of **1a**, **1b**, and **2** (including Lewis structure). **1a**: $d(\text{Cu}-\text{Cu})$: 3.293(8) Å, **1b**: 3.321(1) Å. Ellipsoids are set at the 50% probability level. The counter ions of **1a** and **1b** are omitted for clarity.

determined for both compounds (Figure 1) and resemble comparable structures described in the literature.^[10,12–14,23] Additionally, structure optimization was performed at B3LYP/def2-TZVP level, which showed good geometrical agreement with the experimental results (Figure S47, Table S26 in the Supporting Information).

The structure of **2** resembles that known for nickel(II) ions.^[23–25] Two Hdmg[−] molecules span the pseudo-macrocyclic ligand framework to yield a slightly distorted square-planar coordination geometry for the copper(II) center. The structure of **1** corresponds to that of isomer I (Figure 1). The dimethylglyoxime ligands form distorted square-planar coordination environments for both copper(II) centers, whereas one copper center is coordinated by one Hdmg[−] and one dmg^{2−} molecule, which form a pseudo-macrocyclic coordination environment similar to that in **2**. The pseudo-macrocycle in **1** is, however, not completed by a second proton. Instead, the deprotonated glyoximate residues coordinate the second copper(II) center. An additional H₂dmg ligand completes the square-planar coordination environment. Additionally, one ethanol solvent molecule coordinates one of the copper centers leading to two different isomers **1a** and **1b** with [N₃O₂]/[N₂O₂] and [N₃O]/[N₂O₃] motifs, respectively. **1a** and **1b** (Figure 1, bottom) are found in the same ratio in the crystal structure. In the following, the ratiometric mixture of **1a** and **1b** is referred to as **1**.

Neither isomer II nor III was obtained as solid compound. This experimental result is in agreement with DFT calculations that show that isomer I is the lower energy isomer (Table S26). Further DFT calculations concerning I and II reveal a strong antiferromagnetic exchange coupling of two $S = 1/2$ states, which results in a singlet (broken symmetry state) and a triplet state (Figure 2) in agreement with the experimental results of Ruiz *et al.*^[13,14] The singlet state of I is 5.2 kJ mol^{−1} lower in energy compared to the singlet state of II (Table S26). Isomer III

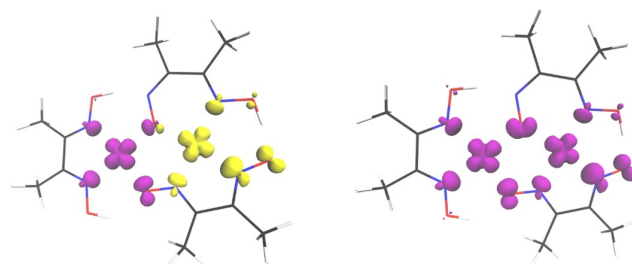


Figure 2. Spin density for singlet (left) and triplet (right) states of isomer I. The isovalue: ± 0.01 , S^2 for singlet is 0.86 (indicating broken-spin solution), for triplet is 2.

was 22.8 kJ mol^{−1} higher in energy than isomer I and was not further considered. In I, the Cu^{II} ions are bridged by the NO-glyoxime groups in a $\mu_2-\eta^1:\eta^1$ (N and O each coordinating one copper center) and $\mu_2-\eta^1$ (O coordinating both copper centers) fashion. In contrast, there are only $\mu_2-\eta^1:\eta^1$ motifs in II. The energy difference between the broken symmetry state and the triplet state is 10 kJ mol^{−1} larger in I. This indicates that the purely O-bridged $\mu_2-\eta^1$ mode dominates the superexchange pathway. However, the calculated singlet triplet gaps also include structural changes and are known to be overestimated by DFT.^[26]

Compounds **1** and **2** were characterized by UV/Vis, IR, MS, EPR, and DFT methods. The UV/Vis spectrum of **1** (Figures S6 and S7) is similar to UV/Vis spectra of comparable compounds^[12–14] and exhibits two strong transitions, 229 and 271 nm, with molar absorption coefficients of approximately 20000 L mol^{−1} cm^{−1}. The band at 229 nm reflects transitions into LC (ligand centered) states as the spectrum of free H₂dmg displays a band at 227 nm ($\epsilon_m = 11302$ L mol^{−1} cm^{−1}). At 435 nm ($\epsilon_m = 2471$ L mol^{−1} cm^{−1}) a weaker absorption maximum is visible, which previously was assigned to transitions into LMCT (ligand-to-metal-charge-transfer) states.^[12–14]

The experimental spectrum is in excellent agreement with the time-dependent (TD) DFT predicted UV/Vis-spectrum that predicted two maxima at 230 and 270 nm and several maxima of lower intensity at higher wavelengths (see the Supporting Information Sections 2, 9.3, and 9.6, Figures S49, S51–S56, and Table S15). The spectroscopic signature of **2** resembles that of **1**, where the main difference is the inversed intensity ratio of the bands at 228 and 275 nm, ($\epsilon_m = 14474$ L mol^{−1} cm^{−1} and $\epsilon_m = 9244$ L mol^{−1} cm^{−1}, respectively) caused by the different coordination modes of the ligands. Additionally, a hypsochromic shift and decreased absorption coefficient of the maximum at 435 to 379 nm ($\epsilon_m = 1854$ L mol^{−1} cm^{−1}) was observed.

The characterization of **1** and **2** by ESI mass spectrometry yielded characteristic signals at mass to charge ratios of 471 for **1** (corresponding to [Cu₂(dmg)(Hdmg)(H₂dmg)]⁺) and 294 for **2**, which corresponds to [2 + H⁺]⁺ (see the Supporting Information Section 3).

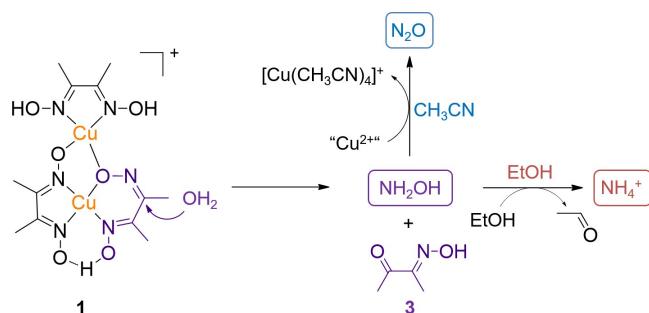
Static FTIR spectra of **1**, **2**, and H₂dmg were recorded in the solid state as KBr pellets with **1** and **2** showing similar vibrational bands. Notably, the CN stretching vibrations are not observed in the spectrum of H₂dmg as a result from a

pronounced impact of the hydrogen bonding.^[17] The assignment of the vibrational bands is discussed in detail in the Supporting Information. It is important to mention that the IR spectrum of **1** in CD₃CN was similar to that in a KBr glass, so that the molecular structure is basically maintained in solution on short timescales (< 1 min; Figure S25).

Compounds **1** and **2** were further analyzed by a qualitative study with X-band EPR spectroscopy (9.5 GHz at 100 K, see the Supporting Information Section 8, Figures S43–S46 as well as the corresponding calculations and simulations in Supporting Information Section 9.7, Figures S59 and S60, Tables S28–S31). These experiments confirmed Cu^{II} centers in axial elongated coordination and indicated that the molecular structure of **1** in the solid state is very likely maintained in solution.

In general, H₂dmg is reported to form rather stable complexes with 3d metal(II/III) ions, such as [Ni(Hdmg)₂],^[23–25] [Cu(Hdmg)₂],^[10] [Co(Hdmg)₂(H₂O)₂],^[27] and [Co(CN)(Hdmg)₂(pyr)].^[28,29] This behavior holds true for **2**, which is stable at air; however, suspensions/solutions of **1** changed color over the course of days, clearly indicating a chemical reaction. Recrystallization of **1** from ethanol/pentane led to red crystals; however, if not separated from the liquid, these crystals dissolved to yield black oil. During this process, the color of the solution changed from red to green and significant amounts of NH₄ClO₄ crystallized (Figure S4). Furthermore, the characteristic and strong odor of acetaldehyde was perceptible. In contrast, when using acetonitrile instead of ethanol, the solution decolorized. Within a day, significant amounts of [Cu(CH₃CN)₄]ClO₄ crystallized (Figure S3). These observations caught our attention. Despite the different reaction outcome, we postulate the same initial reaction step: the nucleophilic attack of H₂O at the glyoxime carbon atom leads to hydrolysis of the Hdmg[−]/dmg^{2−} ligand, which yields butane-2,3-dione monoxime (**3**) and intermediate NH₂OH. Depending on the reaction conditions, NH₂OH was either oxidized to N₂O (yielding Cu⁺ as reduced species) or reduced to NH₄⁺ (yielding acetaldehyde as oxidized species, Scheme 1).

Several spectroscopic and theoretical methods were employed to support this hypothesis. We were able to provide reasonable insight into the reactivity of **1**; however, because of the complexity of the system and the high volatility of diverse



Scheme 1. Postulated nucleophilic attack of H₂O at the glyoxime carbon atom to form intermediate NH₂OH and butane-2,3-dione monoxime (**3**). Depending on the solvent, NH₂OH was either oxidized to N₂O or reduced to NH₄⁺.

reaction products, only a generalized mechanism could be proposed. As a first step, we propose the nucleophilic attack of H₂O at the glyoxime carbon atom of the bridging $\mu_2\text{-}\eta^1\text{-O-N=C}$ -group. Due to this unique coordination to two Lewis acidic centers, the electron density distribution in comparison to the other O–N=C motifs differs. As shown by analysis of the molecular potential and the Mulliken charges of **1**, the electrophilicity at the carbon atom of this glyoximate group is higher than that of the other carbon atoms, facilitating the nucleophilic attack of H₂O (see the Supporting Information Section 9.4).

The presence of this special Cu–O–Cu coordination motif clearly distinguishes **1** from **2**, in which accordingly a nucleophilic attack of water is not favored, thus, leading to the stability of **2** against moisture and water. Consequently, the favored hydrolysis of the Hdmg[−]/dmg^{2−} molecule can be understood as cooperativity of both Cu^{II} ions working together to enable the nucleophilic attack of H₂O. This hydrolysis yields NH₂OH and **3** that could be detected in the reaction solutions (see below). To support this initial step, we carried out DFT calculations that focused on the formation of NH₂OH. The mechanism proposed generally represents an oxime hydrolysis (Figure 3). We observed that the energy barrier of the reaction is strongly dependent on the number of water molecules involved in the process, that is, when just one water molecule is involved, the barrier is much higher. This is consistent with results of Rzepa obtained by using a model system.^[30] The first stage is a nucleophilic attack of H₂O on the most electrophilic carbon atom, which is in the $\mu_2\text{-O-N=C}$ -group (see the Supporting Information Section 9.4.1 and Figure S50, C6). Simultaneously, proton reorganization mediated by a second H₂O molecule takes place at a neighboring oxime group (see TS1 in Figure 3). It is important to note that this proton transfer takes part not from the water molecule, but from the N–OH

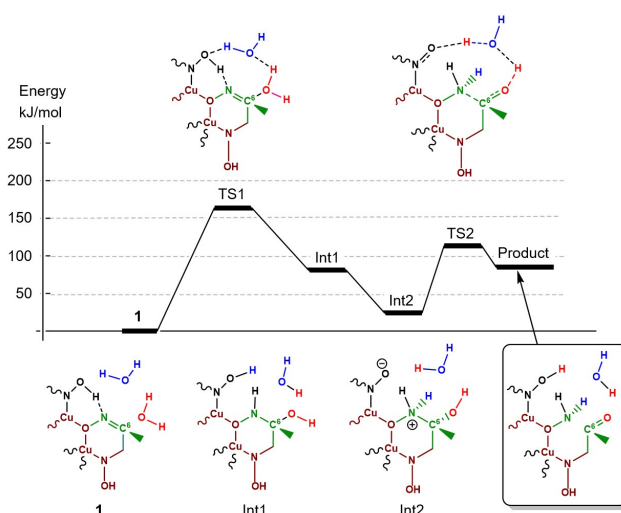


Figure 3. Proposed mechanism and energy diagram for isomer I using B3LYP/def2-TZVP. The atom C6 is labeled because it shows the highest partial charge. The part of the molecule not taking part in the reaction is omitted for clarity. The complete structures are shown in Figure S48.

group of the coordinating oxime (that is reprotonated from the water chain by Grotthuss mechanism).^[31] This results in Intermediate 1 (Int1) that easily turns into a zwitterionic tautomer (Intermediate 2, Int2). The latter tautomerizes with N–C bond splitting into the product, which is a coordinated butane-2,3-dione monoxime (3). Thus, the role of the second H₂O molecule (not spent in the hydrolysis process) is the proton transfer during the reaction. Here, one can expect that this can be significantly influenced by the solvent and its pH value. The first barrier of 163 kJ mol⁻¹ (140 kJ mol⁻¹) is noticeably higher than the second one 119 kJ mol⁻¹ (84 kJ mol⁻¹) and thus is rate-controlling. The numbers in parenthesis include thermodynamic corrections (Table S27). This calculated first barrier is rather high; however, we assume that consideration of further solvent effects would lower the activation barrier.

To underline this mechanism, we carried out ESI mass spectrometry measurements and time-dependent UV/Vis and FTIR experiments. EPR did not prove to be a suitable method because the differentiation of the two Cu^{II} centers was not possible (Supporting Information Section 8).

Reactivity of 1 in ethanol

Time-dependent UV/Vis spectroscopic measurements over a time period of 6 d revealed an increase of the absorption maxima at 229 nm referring to ligand internal transitions into LC states and a decrease of the absorption maximum at 460 nm (Figure 4).

Both of these observations are consistent with the decomposition of 1 and liberation of H₂dmg. Notably, the maximum at 270 nm does not decrease but increases and splits into three maxima (251, 257, and 263 nm) that are hypsochromically shifted. Additionally, two shoulders at 287 and 319 nm formed, whereas the shoulder at 287 nm decreases over time, again. This behavior indicates the degradation of H₂dmg and/or formation of new H₂dmg containing species. We calculated the

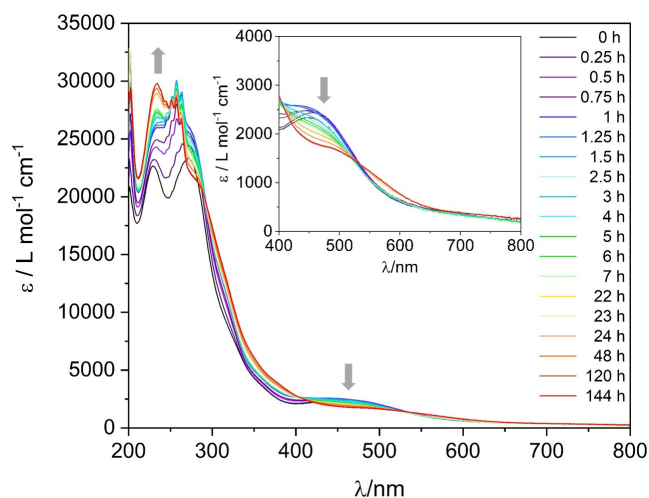


Figure 4. Time-dependent UV/Vis spectra of 1 in ethanol ($c = 3.63 \times 10^{-5} \text{ mol L}^{-1}$) over a time period of 6 d.

UV/Vis spectra of diverse possible intermediates such as free and complexed 3, [Cu(OH)₂(H₂dmg)], and the mixed-valent Cu^{II}/Cu^I species [Cu^ICu^{II}(H₂dmg)(Hdmg)(dmg)] (Figures S51–S56); however, the identification of the new species formed was not possible because the spectra show similar bands of comparable intensity. Lacking the actual compounds for the spectroscopic comparison, it is unlikely that the identification of either one of those species is possible.

Nevertheless, it was possible to trap and analyze evolving acetaldehyde (see the Supporting Information Sections 5.3 and 7.4, Figures S23 and S27–S29), which clearly supports the suggested decomposition pathway and underlines the oxidation of ethanol.

During subsequent experiments that required a higher concentration solution of 1, a strong concentration-dependence of the reaction was observed. For example, a higher concentrated solution ($c = 1.84 \times 10^{-4} \text{ M}$) of 1 in ethanol did not show significant changes over time in the UV/Vis spectra (Figure S9), indicating that the decomposition of 1 only occurs with high excess ethanol. In accordance with these findings, investigations of high concentration solutions of 1 with ESI mass spectrometry did not show any differences within 24 h, either; however, the measurement of a fresh and low concentration sample revealed the complete decomposition of 1 within a few days. The signal of [Cu₂(dmg)(Hdmg)(H₂dmg)]⁺ (m/z 471, Figures S11, S12, S18, and S20) disappeared, instead, several new signals were observed, for example, at m/z 264 that could correspond to the complex [Cu(3)]⁺, in which one molecule of 3 is deprotonated (Figures S18–S20).

This concentration-dependence further was observed in FTIR mechanistic studies, where concentrations of $c \geq 10 \text{ mM}$ were required. The low solubility of 1 in ethanol as well as strong IR absorptions of ethanol in the region of interest (1700–1100 cm⁻¹) precluded measurements directly in ethanol. Thus, 1 was dissolved in deuterated dimethylsulfoxide ([D₆]DMSO, $c = 15 \text{ mM}$) and an excess of ethanol (50 equiv.) was added. However, a reaction between 1 and ethanol was not detected over 1.5 h (Figure S26), either.

In summary, we could detect the main reaction products NH₄ClO₄ and acetaldehyde, the latter by IR and NMR (Figures S23 and S27–S29). Additional to its crystallization, we could detect NH₄⁺ in solution by adding NeBlér's reagent (K₂[HgI₄]), which forms orange colored [Hg₂N]I in the presence of NH₃/NH₄⁺.^[32] In addition, we could detect an intermediate copper(I) species through addition of neocuproine that forms a bright red complex with Cu^I ions, which crystallized from the reaction mixture (Figure S5). Interestingly, 1 can be regenerated by adding new H₂dmg and airing the flask to oxidize Cu^I to Cu^{II}. After some time, the redox reaction and thus, decomposition of 1 starts again, so that we could repeat this cycle four times. Taken together, these findings underline the proposed reaction pathway, in which intermediate NH₂OH is formed by the hydrolysis of H₂dmg. NH₂OH was then reduced to NH₄⁺. The redox partner for this reaction is ethanol that is oxidized to acetaldehyde. This redox reaction is mediated by the copper centers, which can be concluded from the detection of intermediate Cu^I species. Most notably, in this reaction pathway,

NH_2OH is reduced, which is chemically challenging ($\epsilon_0(\text{NH}_3\text{OH}^+/\text{NH}_4^+) = +1.35 \text{ V}^{[33]}$) and therefore usually not observed. NH_2OH is a strong reducing agent and thus, typically is oxidized to N_2 and/or N_2O ($\epsilon_0(\text{NH}_3\text{OH}^+/\text{N}_2, \text{N}_2\text{O}) = -1.87 \text{ V}^{[33]}$). In general, Cu^{II} ions do even catalyze this oxidation.^[34] At high concentrations, NH_2OH tends to disproportionate into NH_3 , N_2 , and N_2O ,^[33] however, that is clearly not the case for the reactivity described within this article. First, we do not observe N_2O as oxidation product, but only acetaldehyde, and second, the reaction does only occur at low concentrations. This observation can be explained by the chemically demanding reaction conditions and the concentration-dependence of the electrochemical potential ($\epsilon_0(\text{EtOH}/\text{acetaldehyde}) = -0.197$ at pH 7).^[35] It is remarkable that NH_2OH is reduced to NH_4^+ under these conditions. In this context, it is interesting to note that even in nature, there are only few enzymes that are capable of the reduction of NH_2OH to NH_4^+ .^[36–40] Among them is the copper containing nitrite reductase (CuNiR),^[39,40] which notably, uses a dinuclear copper-type two-center for substrate activation.^[41]

Reactivity of 1 in acetonitrile

The time-dependent UV/Vis spectra showed bleaching of the solution and accordingly reduction of the dinuclear 1 to $[\text{Cu}(\text{CH}_3\text{CN})_4]^+$ (Figure 5), which can be obtained as crystalline solid in 68% yield from the reaction solution (Figure S3).

The decomposition of 1 is indicated by the increase in intensity of transitions into LC states (204, 230 nm), which corresponds to a rising amount of free H_2dmg . Further evidence for this decomposition and the reduction of Cu^{II} to Cu^{I} is found in the decrease of all other bands. Based on the UV/Vis spectra, this process is completed within 12 h, which indicates a much faster reaction than observed in ethanol. Results of complementary investigations by ESI mass spectrometry match these

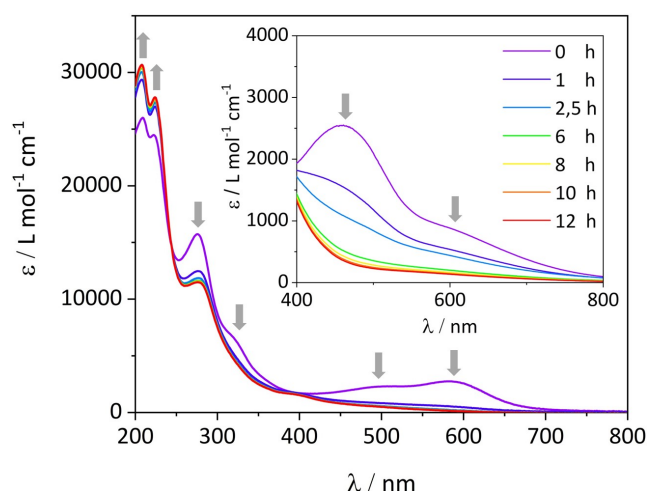


Figure 5. Time-dependent UV/Vis spectra over 12 h of the reaction of 1 in CH_3CN (left: $c = 1.94 \times 10^{-5} \text{ mol L}^{-1}$, right: $c = 7.93 \times 10^{-4} \text{ mol L}^{-1}$). Differences in the spectra for $t = 0 \text{ h}$ derive from the decomposition of 1 that started even in the less-concentrated sample. A comparison with spectra in methanol is given in Figure S8.

findings, where the intensity of the signal of 1 decreases over time and the intensity of the signals of $[\text{Cu}(\text{CH}_3\text{CN})]^+$ (m/z 104) and $[\text{Cu}(\text{CH}_3\text{CN})_2]^+$ (m/z 145) increase. Additionally, several signals that correspond to diverse copper dimethylglyoxime fragments appeared over time, which further underlines the decomposition of 1 (Tables S19 and S20, Figures S14–S17).

The according FTIR investigations were performed in dry CD_3CN over 8 h; however, it was not possible to eliminate all traces of H_2O . In contrast to the observations in $[\text{D}_6]\text{DMSO}$ with ethanol, significant spectral changes were observed already after few minutes (Figure 6).

Hereby, the most important observation is the appearance of a strong new band at 1693 cm^{-1} , which was assigned to a CO stretching vibration and gives a first indication for the formation of 3. This assignment is confirmed by the presence of the same absorption band in the reference IR spectrum of 3 in CD_3CN (Figures S30, S32, and S33). Next to this, a weak band was observed at 2229 cm^{-1} , congruent with the reference of N_2O in CD_3CN (and DMSO, Figure S31), which confirms the suggested product formation (inset in Figure 7, Figure S34). The spectral region of $1650\text{--}1180 \text{ cm}^{-1}$ is discussed in the Supporting Information, with a focus on the conceivable species $[\text{Cu}(\text{CH}_3\text{CN})_4]^+$, H_2dmg , NO_2^- and NO_3^- , the two later ones being present at most as side products. (see the Supporting Information Sections 7.2 and 7.5) In addition to these descriptions, the experimental IR spectra of 1 and 3 are well described by theoretical IR spectra obtained by geometry optimizations and subsequent frequency calculations at DFT level (Figures S41 and S42).

Even though the intrinsic traces of H_2O seemed to be sufficient to initiate the decomposition of 1, we repeated the experiment by adding an excess of H_2O (20 equiv.). Interestingly, the reaction and its kinetics are not significantly influenced during the first hour of the reaction (Figure S39). At longer timescales, however, a follow-up reaction that might relate to complex formation of 3, solvated Cu^{III} ions, and H_2O takes place (see the Supporting Information Section 7.6). To

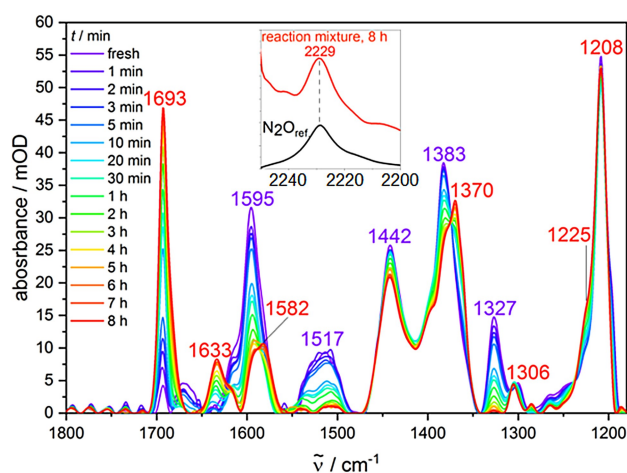


Figure 6. Time-dependent FTIR spectra over 8 h of the reaction of 1 in CD_3CN . The inset is an enlargement of the region around 2230 cm^{-1} (red: reaction mixture after 8 h, black: reference IR spectrum of N_2O in CD_3CN).

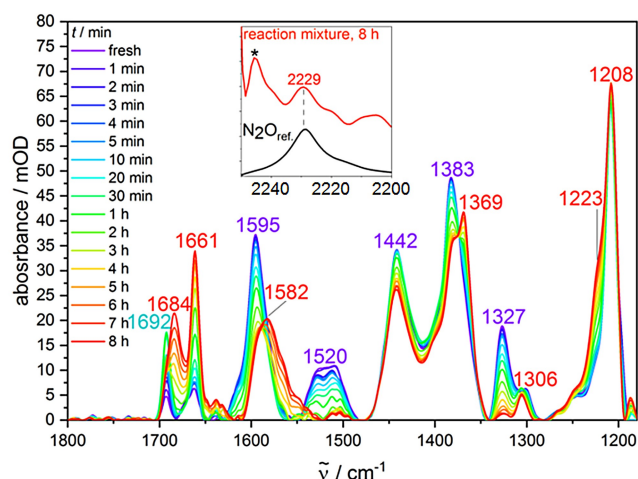


Figure 7. Time-dependent FTIR spectra over 8 h of the reaction of **1** in CD_3CN containing H_2^{18}O (20 equiv.). The inset is an enlargement of the region around 2230 cm^{-1} (red: reaction mixture after 8 h, black: reference IR spectrum of N_2O in CD_3CN). The band marked with an asterisk is an artifact resulting from the strong absorption of CD_3CN in this spectral region.

gain further insight into the mechanism, we carried out experiments with isotopically labeled H_2^{18}O . Based on the proposed mechanism, hydrolysis of H_2dmg would lead to **3**, in which the oxygen atom of the carbonyl function is that of the initially attacking H_2O molecule. Thus, FTIR spectroscopy on **1** in CD_3CN with addition of H_2^{18}O was an ideal tool to experimentally verify this stated mechanism, as the isotope labeled H_2^{18}O should induce a red-shift of the CO stretching vibration by about 40 cm^{-1} (C^{16}O vs. C^{18}O). Indeed, an additional band appeared at 1661 cm^{-1} , which is assigned to the C^{18}O stretching vibration (Figure 7). However, this C^{18}O band coexists with the C^{16}O peak described earlier, which should result from traces of H_2^{16}O that are intrinsically contained in the reaction mixture (despite the use of dry CD_3CN). A more surprising observation is that the C^{16}O signal is stronger than the C^{18}O peak over the first hour of the reaction. This is an indication for preorganized (coordinated) H_2^{16}O molecules that might be present in the solid sample of **1**. Nevertheless, the presence of two distinct CO stretching vibrations (C^{16}O at 1692 cm^{-1} and C^{18}O at 1661 cm^{-1}) clearly strengthens the suggested mechanism. As the C^{16}O peak is logically weaker compared to the investigations without isotope labeled H_2O , the CO stretching vibration attributed to the complexation of formed **3** (see above) is clearly observable as a separate peak at 1684 cm^{-1} . In this particular case, it is only visible as shoulder in the H_2^{16}O experiments. However, it is to mention that in all experiments, the Gaussian deconvolution yielded very similar wavenumbers for the CO vibration of the new species with complexed **3** ($1679\text{--}1682\text{ cm}^{-1}$, Figures S38–S40). The absence of any specific “ ^{18}O band” for this particular vibration might result from similar spectral frequencies of the underlying vibrational modes independent of the isotope (^{16}O or ^{18}O).

In summary, we could detect the main reaction products $[\text{Cu}(\text{CH}_3\text{CN})_4]\text{ClO}_4$, **3**, and N_2O . This finding is in accordance with

the usually observed oxidation of NH_2OH to N_2O ,^[33] which is known to be even catalyzed by Cu^{II} ions.^[34] Furthermore, we could show that the initial step indeed is the nucleophilic attack of H_2O to form **3** and presumably NH_2OH ; however, despite much effort, we were not able to detect intermediate NH_2OH . It is very likely that the nascent NH_2OH is too rapidly oxidized to N_2O to be detected by room-temperature FTIR. Based on the results of the UV/Vis measurements and the good experimental yield of $[\text{Cu}(\text{CH}_3\text{CN})_4]\text{ClO}_4$ (68%), we assume that the decomposition of **1** is rather complete.

Conclusion

We have synthesized and thoroughly characterized the dinuclear copper(II) complex $[\text{Cu}_2(\text{H}_2\text{dmg})(\text{Hdmg})(\text{dmg})]\text{ClO}_4$ (**1**) and its mononuclear analogue $[\text{Cu}(\text{Hdmg})_2]$ (**2**). Three possible coordination isomers I–III of **1** exist; however, based on the spectroscopic signature^[13] and temperature-dependent UV/Vis measurements (see the Supporting Information Section 2.6), we assume that isomer I is dominant. Furthermore, based on the poor match of the calculated and experimental IR spectra, the presence of III is very unlikely (Figure S41).

We found that **1** is sensitive to hydrolysis; this is a result of the cooperative effect of the two Cu^{II} ions, which increases the electrophilia of the glyoxime carbon atom of the bridging $\mu_2\text{-O-N=C}$ -group. DFT calculations reveal a much higher Mulliken charge in comparison to any other carbon atom in the molecule. Therefore, the nucleophilic attack of H_2O is favored at this $\text{Hdmg}^-/\text{H}_2\text{dmg}$ ligand, and this leads to the hydrolysis products butane-2,3-dione monoxime (**3**) and NH_2OH . Depending on the solvent, NH_2OH is either oxidized or reduced. In CH_3CN , NH_2OH is *oxidized* to N_2O , which is in accordance with NH_2OH being a strong reducing agent. The reduction product is $[\text{Cu}(\text{CH}_3\text{CN})_4]\text{ClO}_4$, which crystallizes from the reaction mixture. In contrast, in ethanol, NH_2OH is *reduced* to NH_4^+ , which is obtained in significant amounts as NH_4ClO_4 . The redox partner is ethanol, which is oxidized to acetaldehyde. Based on DFT calculations, we suggest a reaction pathway that is basically glyoxime hydrolysis that yields **3** and NH_2OH . Two H_2O molecules participate in the proposed mechanisms; one nucleophilically attacks the carbon atom and the other one is involved in proton transfer. Even though it was not possible to detect NH_2OH itself and the calculated activation barrier is rather high, the combined approach of theoretical methods, experimental detection and characterization techniques, time-dependent UV/Vis and FTIR spectroscopy, and mass spectrometry allowed the detection of all the main reaction products and thus, underlines the reaction pathway proposed. FTIR spectroscopic measurements with isotopically labeled H_2^{18}O proved the nucleophilic attack of H_2O as initial reaction step.

The possibility of **1** to either oxidize or reduce NH_2OH is remarkable because the electrochemical potentials of both reactions are far apart ($\epsilon_0(\text{NH}_3\text{OH}^+/\text{N}_2, \text{N}_2\text{O}) = -1.87\text{ V}$ and $\epsilon_0(\text{NH}_3\text{OH}^+/\text{NH}_4^+) = +1.35\text{ V}$).^[33] In particular, the reduction of NH_2OH is chemically challenging; this is mirrored by a strong concentration dependence of the hydrolysis of **1** in ethanol. As

a result of the concentration dependence of the electrochemical potential, hydrolysis of **1** with subsequent reduction of NH_2OH to NH_4^+ is only observed at low concentrations/high excess of ethanol.

Experimental Section

Materials and methods: All chemicals used were of p.a. quality and were purchased from Acros Organics, Alfa Aesar, Merck, Roth or Sigma Aldrich if not mentioned otherwise. Solvents for synthesis were degassed but not dried. For time-dependent FTIR spectroscopy, acetonitrile was dried according to literature procedures.^[42] The handling and preparation of air sensitive compounds were performed under a nitrogen atmosphere. Standard Schlenk techniques were used. If not mentioned otherwise all syntheses were performed under inert atmosphere. Analytical data and device parameters (UV/Vis spectroscopy, NMR spectroscopy, IR spectroscopy including corresponding simulations and additional discussion,^[43–48] SC-XRD,^[49–55] elemental analysis, ESI mass spectrometry including corresponding simulations,^[56] and EPR spectroscopy) are given in the Supporting Information.

Deposition Numbers 2203267 (for **1**), 2203268 (for **2**), 2203269 (for $[\text{Cu}(\text{CH}_3\text{CN})_4]\text{ClO}_4$), 2203270 (for $[\text{Cu}(\text{neocuproine})_2]\text{ClO}_4$) contain the supplementary crystallographic data for this paper. These data are provided free of charge by the joint Cambridge Crystallographic Data Centre and Fachinformationszentrum Karlsruhe Access Structures service.

Computational details: All calculations were performed with the program package TURBOMOLE^[45] using density functional theory (DFT). Single-point energy calculations were carried out using tolerances of 10^{-7} Hartrees for the SCF energy change, and default convergence criteria for the geometry optimization. All calculations were performed with the B3LYP functional,^[57–59] def2-TZVP basis set,^[60] and the resolution of the identity (RI) approximation.^[61–63] UV/Vis spectra were calculated with time dependent DFT (TDDFT).^[64,65] Transition states were preoptimized by a reaction path search from Plessow^[66] and then determined by trust region image optimizations.^[67] Solvent effects were not considered. Additionally, computations using the state average complete active space self-consistent field (CASSCF) were done.^[68] With a program developed in Karlsruhe and Kaiserslautern,^[69] spin orbit configuration interaction (SOC) calculations were carried out on the basis of the CASSCF orbitals using a spin orbit mean field technique for the two-electron spin-orbit integrals.^[70,71] The Abragam-Bleaney tensor, as described by Gerloch and McMeeking,^[72] was used to generate the g-tensors (Supporting Information Section 9.7).^[73]

Preparation of $[\text{Cu}_2(\text{H}_2\text{dmg})(\text{Hdmg})(\text{dmg})(\text{EtOH})]\text{ClO}_4$ (1**):** $\text{Cu}(\text{ClO}_4)_2 \cdot 6\text{H}_2\text{O}$ (185 mg, 0.499 mmol) was dissolved in ethanol (ca. 10 mL). H_2dmg (127 mg, 1.09 mmol) was added to the stirred solution. The solution turned deep red and was stirred for 15 min at room temperature. The product could be collected as deep red crystals by pentane diffusion (65 mg, 0.11 mmol, 44 %).

Preparation of $[\text{Cu}(\text{Hdmg})_2]$ (2**):** Synthetic procedure using $\text{Cu}(\text{OAc})_2 \cdot 2\text{H}_2\text{O}$: According to literature^[10] $\text{Cu}(\text{OAc})_2 \cdot 2\text{H}_2\text{O}$ (101 mg, 0.506 mmol) was dissolved in methanol (ca. 20 mL). H_2dmg (117 mg, 1.01 mmol) in methanol (ca. 20 mL) was added to the stirred solution of the salt. The solution turned deep red and was stirred for 30 min at room temperature. After slow evaporation of the solvent in air, the product could be collected as red crystals (62 mg, 0.21 mmol, 42 %).

Preparation of $[\text{Cu}(\text{CH}_3\text{CN})_4]\text{ClO}_4$: $\text{Cu}(\text{ClO}_4)_2 \cdot 6\text{H}_2\text{O}$ (182 mg, 0.491 mmol) was dissolved in acetonitrile (ca. 15 mL). H_2dmg

(124 mg, 1.07 mmol) was added to the stirred solution. The solution turned deep green. The product was obtained as colorless crystals by diethyl ether diffusion (109 mg, 0.333 mmol, 68 %). Among the crystallization process, the solution decolorized.

Acknowledgements

The authors gratefully acknowledge the financial support from TRR/SFB 88 “3MET”. S. B. and R. I. P. thank Dr. Jonathan Becker (JLU Giessen) for his support in crystal measurement. E. B. and K. F. acknowledge support by the state of Baden-Württemberg through bwHPC and the German Research Foundation (DFG) through grant no. INST 40/575-1 FUGG (JUSTUS 2 cluster). Open Access funding enabled and organized by Projekt DEAL.

Conflict of Interest

The authors declare no conflict of interest.

Data Availability Statement

The data that support the findings of this study are available in the supplementary material of this article.

Keywords: cooperative effects · copper complexes · dimethylglyoxime · hydrolysis · hydroxylamine

- [1] N. Sträter, W. N. Lipscomb, T. Klabunde, B. Krebs, *Angew. Chem. Int. Ed. Engl.* **1996**, *35*, 2024–2055.
- [2] B. Bosnich, *Inorg. Chem.* **1999**, *38*, 2554–2562.
- [3] J. I. van der Vlugt, *Eur. J. Inorg. Chem.* **2012**, *2012*, 363–375.
- [4] P. Buchwalter, J. Rosé, P. Braunstein, *Chem. Rev.* **2015**, *115*, 28–126.
- [5] L. Tebben, C. Mück-Lichtenfeld, G. Fernández, S. Grimme, A. Studer, *Chem. Eur. J.* **2017**, *23*, 5864–5873.
- [6] M. H. Proscenc, M. M. Kappes, G. Niedner-Schatteburg, *Chem. Eur. J.* **2021**, *27*, 15019–15020.
- [7] T. Wall, M. Leist, F. Dietrich, W. R. Thiel, M. Gerhards, *ChemPlusChem* **2021**, *86*, 622–628.
- [8] M. Grupe, P. Boden, P. Di Martino-Fumo, X. Gui, C. Bruschi, R. Israil, M. Schmitt, M. Nieger, M. Gerhards, W. Klopffer, C. Riehn, C. Bizzarri, R. Diller, *Chem. Eur. J.* **2021**, *27*, 15252–15271.
- [9] Transregional collaborative research center located at the TU Kaiserslautern (TUK) and Karlsruhe Institute of Technology (KIT), **2009–2022**.
- [10] E. Frasson, R. Bardi, S. Bezzi, *Acta Crystallogr.* **1959**, *12*, 201–205.
- [11] D. H. Svedung, *Acta Chem. Scand.* **1969**, *23*, 2865–2878.
- [12] R. I. Petrikat, S. Becker, *Z. Anorg. Allg. Chem.* **2022**, *648*, e202200150.
- [13] R. Ruiz, J. Sanz, B. Cervera, F. Lloret, M. Julve, C. Bois, J. Faus, M. C. Muñoz, *J. Chem. Soc. Dalton Trans.* **1993**, 1623–1628.
- [14] R. Ruiz, J. Sanz, F. Lloret, M. Julve, J. Faus, C. Bois, M. C. Muñoz, *J. Chem. Soc. Dalton Trans.* **1993**, 3035–3039.
- [15] X.-Y. Chen, P. Cheng, X.-W. Liu, S.-P. Yan, W.-M. Bu, D.-Z. Liao, Z.-H. Jiang, *Chem. Lett.* **2003**, *32*, 118–119.
- [16] C.-H. Li, R.-J. Wang, H.-Z. Kou, Y.-D. Li, *Inorg. Chem. Commun.* **2002**, *5*, 403–406.
- [17] P. K. Panja, S. Bala, C. Pal, P. N. Ghosh, *J. Mol. Struct.* **1991**, *249*, 277–283.
- [18] J. E. Caton, Jr., C. V. Banks, *Talanta* **1966**, *13*, 967–977.
- [19] K. E. Falk, E. Ivanova, B. Roos, T. Vanngard, *Inorg. Chem.* **1970**, *9*, 556–562.
- [20] X. Wu, W. Hu, *Chin. J. Chem.* **2011**, *29*, 2124–2128.
- [21] K. Xavier, *Appl. Catal.* **2004**, *258*, 251–259.

- [22] C. Gawlig, S. Schindler, S. Becker, *Eur. J. Inorg. Chem.* **2020**, 2020, 248–252.
- [23] L. Tschugaeff, *Ber. Dtsch. Chem. Ges.* **1905**, 38, 2520–2522.
- [24] P. Pfeiffer, *Ber. Dtsch. Chem. Ges. A* **1930**, 63, 1811–1816.
- [25] L. E. Godycki, R. E. Rundle, R. C. Voter, C. V. Banks, *J. Chem. Phys.* **1951**, 19, 1205–1206.
- [26] G. Singh, S. Gamboa, M. Orio, D. A. Pantazis, M. Roemelt, *Theor. Chem. Acc.* **2021**, 140, 139.
- [27] G. N. Schrauzer, R. J. Windgassen, *Chem. Ber.* **1966**, 99, 602–610.
- [28] G. N. Schrauzer, J. Kohnle, *Chem. Ber.* **1964**, 97, 3056–3064.
- [29] G. N. Schrauzer, *Acc. Chem. Res.* **1968**, 1, 97–103.
- [30] H. S. Rzepa, in *Henry Rzepa's Blog*, "Oxime formation from hydroxylamine and ketone", can be found under <https://www.ch.imperial.ac.uk/rzepa/blog/?p=7822>, **2012**.
- [31] N. Agmon, *Chem. Phys. Lett.* **1995**, 244, 456–462.
- [32] J. Nessler, *Über das Verhalten des Jodquecksilbers und der Quecksilberverbindungen, überhaupt zu Ammoniak und über eine neue Reaktion auf Ammoniak*, Albert-Ludwigs-Universität, Freiburg, **1856**.
- [33] A. F. Holleman, E. Wiberg, N. Wiberg, in *Lehrbuch der anorganischen Chemie*, De Gruyter, Berlin, **1985**.
- [34] J. H. Anderson, *Analyst* **1964**, 89, 357.
- [35] D. Voet, J. G. Voet, C. W. Pratt, in *Lehrbuch der Biochemie*, Wiley-VCH, Weinheim, **2019**.
- [36] R. Sturms, A. A. DiSpirito, D. B. Fulton, M. S. Hargrove, *Biochemistry* **2011**, 50, 10829–10835.
- [37] J. Singh, *Biochim. Biophys. Acta Bioenerg.* **1974**, 333, 28–36.
- [38] O. Einsle, A. Messerschmidt, R. Huber, P. M. H. Kroneck, F. Neese, *J. Am. Chem. Soc.* **2002**, 124, 11737–11745.
- [39] J. Simon, P. M. H. Kroneck, in *The Metal-Driven Biogeochemistry of Gaseous Compounds in the Environment* (Eds.: P. M. H. Kroneck, M. E. S. Torres), Springer, Dordrecht, **2014**, pp. 211–236.
- [40] P. M. Harrison, in *Metalloproteins. 1: Metal Proteins with Redox Roles*, Verlag Chemie, Weinheim, **1985**.
- [41] M. Sundararajan, I. H. Hillier, N. A. Burton, *J. Phys. Chem. B* **2007**, 111, 5511–5517.
- [42] J. F. Coetzee, *Pure Appl. Chem.* **1966**, 13, 427–436.
- [43] M. J. Frisch, G. W. Trucks, H. W. Schlegel, G. E. Scuseria, M. A. Robb, J. R. Cheeseman, G. Scalmani, V. Barone, G. A. Petersson, H. Nakatsuji, X. Li, M. Caricato, A. Marenich, J. Bloino, B. G. Janesko, R. Gomperts, B. Mennucci, H. P. Hratchian, J. V. Ortiz, A. F. Izmaylov, J. L. Sonnenberg, D. Williams-Young, F. Ding, F. Lipparini, F. Egidi, J. Goings, B. Peng, A. Petrone, T. Henderson, D. Ranasinghe, V. G. Zakrzewski, J. Gao, N. Rega, G. Zheng, W. Liang, M. Hada, M. Ehara, K. Throssell, J. A. Montgomery, Jr., J. E. Peralta, F. Ogliaro, M. Bearpark, J. J. Heyd, E. Brothers, K. N. Kudin, V. N. Staroverov, T. Keith, R. Kobayashi, J. Normand, K. Raghavachari, A. Rendell, J. C. Burant, S. S. Iyengar, J. Tomasi, M. Cossi, J. M. Millam, M. Klene, C. Adamo, R. Cammi, J. W. Ochterski, R. L. Martin, K. Morokuma, O. Farkas, J. B. Foresman, D. J. Fox, *Gaussian 09*, Gaussian Inc., Wilford, CT, **2016**.
- [44] F. Furche, R. Ahlrichs, C. Hättig, W. Klopper, M. Sierka, F. Weigend, *WIREs Comput. Mol. Sci.* **2014**, 4, 91–100.
- [45] a) TURBOMOLE V7.5 **2020**, a development of University of Karlsruhe and Forschungszentrum Karlsruhe GmbH, 1989–2007, TURBOMOLE GmbH, since **2007**; available from <https://www.turbomole.org>; b) S. G. Balasubramani, G. P. Chen, S. Coriani, M. Diedenhofen, M. S. Frank, Y. J. Franzke, F. Furche, R. Grotjahn, M. E. Harding, C. Hättig, A. Hellweg, B. Helmich-Paris, C. Holzer, U. Huniar, M. Kaupp, A. Marefat Khah, S. Karbalaei Khani, T. Müller, F. Mack, B. D. Nguyen, S. M. Parker, E. Perlt, D. Rappoport, K. Reiter, S. Roy, M. Rückert, G. Schmitz, M. Sierka, E. Tapavicza, D. P. Tew, C. van Wüllen, V. K. Voora, F. Weigend, A. Wodyński, J. M. Yu, *J. Chem. Phys.* **2020**, 152, 184107.
- [46] S. Grimme, J. Antony, S. Ehrlich, H. Krieg, *J. Chem. Phys.* **2010**, 132, 154104.
- [47] S. Grimme, S. Ehrlich, L. Goerigk, *J. Comput. Chem.* **2011**, 32, 1456–1465.
- [48] R. Blinc, D. Hadži, *J. Chem. Soc.* **1958**, 4536–4540.
- [49] L. Krause, R. Herbst-Irmer, G. M. Sheldrick, D. Stalke, *J. Appl. Crystallogr.* **2015**, 48, 3–10.
- [50] APEX2, Bruker AXS, Inc., Madison, WI, USA.
- [51] XPREP, Bruker AXS, Inc., Madison, WI, USA.
- [52] G. M. Sheldrick, *Acta Crystallogr. Sect. A* **2015**, 71, 3–8.
- [53] G. M. Sheldrick, *Acta Crystallogr. Sect. C* **2015**, 71, 3–8.
- [54] C. B. Hübschle, G. M. Sheldrick, B. Dittrich, *J. Appl. Crystallogr.* **2011**, 44, 1281–1284.
- [55] A. L. Spek, *Platon*, University of Utrecht (The Netherlands), **2008**.
- [56] M. Loos, C. Gerber, F. Corona, J. Hollender, H. Singer, *Anal. Chem.* **2015**, 87, 5738–5744.
- [57] A. D. Becke, *J. Chem. Phys.* **1993**, 98, 5648–5652.
- [58] A. D. Becke, *Phys. Rev. A* **1988**, 38, 3098–3100.
- [59] C. Lee, W. Yang, R. G. Parr, *Phys. Rev. B* **1988**, 37, 785–789.
- [60] F. Weigend, R. Ahlrichs, *Phys. Chem. Chem. Phys.* **2005**, 7, 3297–3305.
- [61] K. Eichkorn, O. Treutler, H. Öhm, M. Häser, R. Ahlrichs, *Chem. Phys. Lett.* **1995**, 240, 283–290.
- [62] K. Eichkorn, F. Weigend, O. Treutler, R. Ahlrichs, *Theor. Chem. Acta* **1997**, 97, 119–124.
- [63] F. Weigend, *Phys. Chem. Chem. Phys.* **2006**, 8, 1057–1065.
- [64] R. Bauernschmitt, R. Ahlrichs, *Chem. Phys. Lett.* **1996**, 256, 454–464.
- [65] R. Bauernschmitt, M. Häser, O. Treutler, R. Ahlrichs, *Chem. Phys. Lett.* **1997**, 264, 573–578.
- [66] P. Plessow, *J. Chem. Theory Comput.* **2013**, 9, 1305–1310.
- [67] T. Helgaker, *Chem. Phys. Lett.* **1991**, 182, 503–510.
- [68] U. Meier, V. Staemmler, *Theor. Chim. Acta* **1989**, 76, 95–111.
- [69] T. Bodenstein, A. Heimermann, K. Fink, C. van Wüllen, *ChemPhysChem* **2022**, 23, e202100648.
- [70] F. Neese, *J. Chem. Phys.* **2005**, 122, 034107.
- [71] B. Helmich-Paris, C. Hättig, C. van Wüllen, *J. Chem. Theory Comput.* **2016**, 12, 1892–1904.
- [72] M. Gerloch, R. F. McMeeking, *J. Chem. Soc. Dalton Trans.* **1975**, 2443.
- [73] R. Selwin Joseyphus, M. Sivasankaran Nair, *Arab. J. Chem.* **2010**, 3, 195–204.

Manuscript received: November 5, 2022

Accepted manuscript online: February 20, 2023

Version of record online: March 20, 2023